Silica-Sheathed Pyrrotite Nanowires: Synthesis and Mechanism

Hao-Xu Zhang,[†,‡] Jian-Ping Ge,[†] Jin Wang,[†] Zhe Wang,[§] Da-Peng Yu,[§] and Ya-Dong Li*[,†]

Department of Chemistry, The Key Laboratory of Atomic and Molecular Nanoscience (Ministry of Education), Tsinghua University, National Center for Nanoscience and Nanotechnology, Beijing 100084, People's Republic of China, Nanoscale Physics and Devices Laboratory, Institute of Physics, Chinese Academy of Sciences, Beijing 100080, People's Republic of China, and State Key Laboratory for Mesoscopic Physics and Electron Microscopy Laboratory, School of Physics, Peking University, Beijing 100871, People's Republic of China

Received: March 5, 2005; In Final Form: April 18, 2005

We have studied the growth of silica-sheathed 3C-Fe_7S_8 products on silicon substrates with $FeCl_2$ and sulfur precursors at the temperature region of 600−800 °C. On the basis of the crystal structure of Fe_7S_8, we have proposed a model including the kinetic competition of the adsorption of silica species on Fe2−Fe3−Fe4 units at the 4Fe layer and on the Fe2−Fe3−Fe4−Fe5 units parallel to the *c*-axis. Using this model, we have not only explained all the experimental phenomena but also especially prepared Fe_7S_8 nanowires at 650 °C by introducing water into the reaction system.

Introduction

As is well-known, to control the sizes and shapes of nanostructured materials is an effective way to tailor their chemical and physical properties. Therefore we have witnessed growing efforts toward this utmost goal in the past decade.[1−4] To achieve this, better understanding on the growth behavior of a material and its interaction with another material, which serves as a template, is substantial. Here our topic material is a kind of iron sulfide, Fe_7S_8. Iron sulfides, as low cost and low toxic materials with interesting electrical[5,6] and magnetic[5d,e,7] properties and potential applications,[6a,8,9] have aroused great efforts on their synthesis via various approaches in solution systems[10,11] or through vapor phase.[12,13] However as is well-known, the Fe−S system has such a complex phase diagram that a series of pyrrotite ($Fe_{1-x}S$) compositions occur between troilite (FeS) and pyrite (FeS_2), apart from the sulfur deficient type of marchinawite (FeS_{1-x}) and the metastable greigite (Fe_3S_4). Thus the attempts to prepare their nanometer-sized products with pure phases may encounter great problems. And it was only in the past year that the pyrrotite nanowires had been synthesized for the first time.[10a] So it is important to explore new methods for synthesis of pyrrotite nanowires and to study the formation mechanism.

Recently we have developed a general atmospheric pressure chemical vapor deposition (APCVD) route to synthesize silica-sheathed metal sulfide nanowires on silicon wafers with metal chlorides and sulfur as the precursors.[12b,14] In ref 12b we have tried to give a general explanation about the growth mechanism of some of the nanowires basing on Bravais' law, that is, on the basis of the inherent growth behavior of the sulfide crystals. However the existence of the silica sheath may indicate the template-directed growth as an alternative mechanism. Particularly we notice Xie's report on the synthesis of hexagonal Fe_7S_8 platelike microcrystals,[10b] which shows that the *c*-axis is not the favored growth direction, seeming to be in contradiction with our results. Therefore it is necessary to conduct systematic studies on the preparation of pyrrotite nanowires. In this paper, we report our colorful results and demonstrate the template-directed growth as the dominating mechanism.

Experimental Section

The preparation of silica-sheathed Fe_7S_8 nanowires was carried out in a quartz tube, which was placed in a 36 cm long horizontal tube furnace with a typical bell-shaped temperature profile. The temperature profile of the furnace is shown as Figure 9 in ref 12b. $FeCl_2 \cdot 4H_2O$ and sulfur (A.R. reagents from the Beijing Chemical Factory, China) were used as purchased. $FeCl_2 \cdot 4H_2O$ was selected as the iron source instead of $FeCl_3$ because it loses all the water below 200 °C and the pure phase of Fe_7S_8 can be obtained with it; see Electronic Supporting Information (ESI). Two graphite boats with the length of 2 cm were used to contain the precursors. Several Si(100) substrates contained in alumina boats were put at the downstream side. We first evacuated the quartz tube with a rotary pump, then enhanced the furnace temperature to 150 °C in 10 min, and further enhanced it to 200 °C in the next 20 min. After that, we stopped the evacuation and filled the system with argon. In the next 30 min the furnace temperature was enhanced to a predetermined temperature. And deposition was conducted under an argon flow of 60 cm^3(STP) min^{-1}. At last the furnace was allowed to naturally cool to room temperature before the samples were taken out. Details for the preparation of the samples introduced in this paper are summarized in Table 1.

The samples were characterized by a Bruker D8 Advance X-ray diffractmeter (XRD) with Cu Kα radiation ($\lambda = 1.5418$ Å). The size and morphology of the samples were obtained with scanning electron microscopes (SEMs, including LEO-1530 and JSM-6301F) and transmission electron microscopes (TEMs, including Hitachi H-800, JEM-1200EX, JEOL-2010F, and Philips Tecnai-F30).

General Results

SEM I. SEM results of a series of samples (Nos. 1−5) prepared at different temperatures (600−800 °C) are sum-

* To whom correspondence should be addressed. E-mail: ydli@tsinghua.edu.cn.
† Tsinghua University.
‡ Chinese Academy of Sciences.
§ Peking University.

10.1021/jp051142o CCC: $30.25
Published on Web 05/19/2005

TABLE 1: Parameters for the APCVD of the Samples

sample	substrate (cm)	$FeCl_2 \cdot 4H_2O$ (cm)	sulfur (cm)	furnace temp (°C)
1	3.0 to 4.0	6.0 to 8.0 (0.40 g)	15.2 to 17.2	600
2	3.0 to 4.0	6.0 to 8.0 (0.40 g)	15.6 to 17.6	650
3	3.0 to 4.0	6.0 to 8.0 (0.40 g)	15.9 to 17.9	700
4	3.0 to 4.0	6.0 to 8.0 (0.40 g)	16.2 to 17.2	750
5	3.0 to 4.0	6.0 to 8.0 (0.40 g)	16.5 to 18.5	800
6	−7.0 to −6.0	6.0 to 8.0 (0.40 g)	15.9 to 17.9	700
7	3.0 to 4.0	6.0 to 8.0 (1.00 g)	16.2 to 17.2	750
8	−7.0 to −6.0	10.0 to 12.0 (1.00 g)	16.5 to 18.5	800
9[a]	3.0 to 4.0	6.0 to 8.0 (0.40 g)	15.6 to 17.6	650
10	−11.5 to −10.5	10.5 to 12.5 (0.70 g) 7.0 to 8.0 (0.10 g)	16.5 to 18.5	800

[a] Leaking water (18 °C) vapor into the system through a i.d. 1.2 mm hole. The $FeCl_2$ precursor is prevented from having direct exposure to water vapor by putting it in a one-side sealed tube.

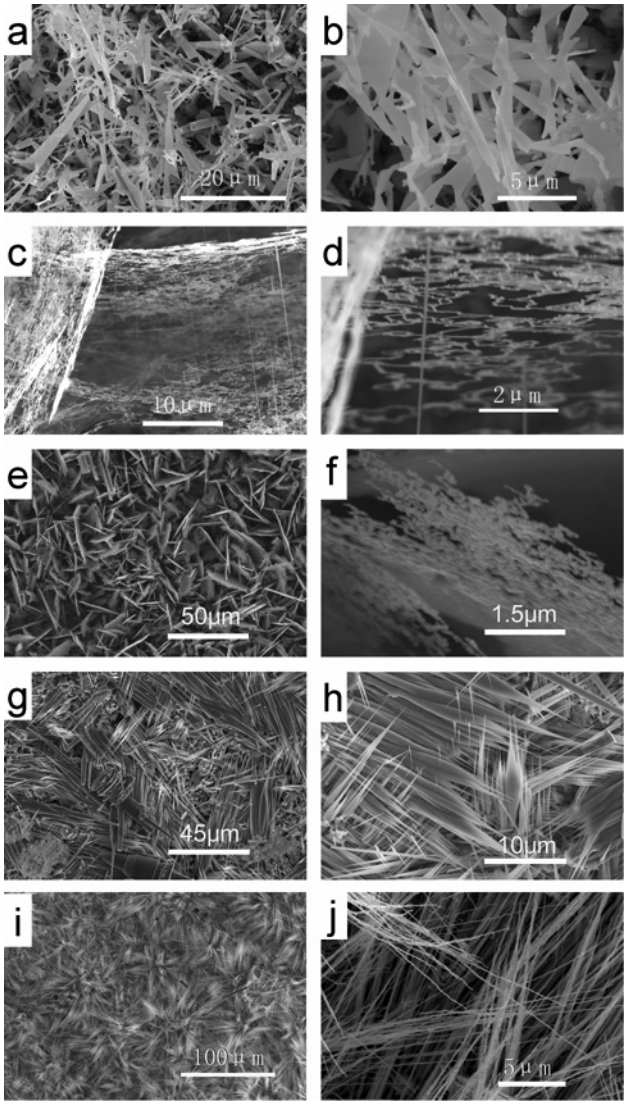

Figure 1. SEM images of samples 1−5 prepared at (a) 600, (c) 650, (e) 700, (g) 750, and (i) 800 °C. Higher resolution images of these samples are shown as b, d, f, h, and j, respectively.

marized in Figure 1. Parts a−f of Figure 1 show that the samples prepared at 600, 650, and 700 °C all have beltlike network products but with some differences. One is that such belts turn to be much more narrow in the 650 and 700 °C samples than in the 600 °C sample. And the other is that in the 700 °C sample the beltlike networks not only appear at the edges of the sheetlike products but also grow exactly at the same planes with the sheets they originated from. In addition much more nanowires have appeared in the 650 °C sample, in comparison with the 600 °C sample. In high contrast with the beltlike or sheetlike products obtained at 600−700 °C, the 750 and 800 °C samples (see Figure 1g−j) are covered with wirelike products appearing as bundles. The main difference between the two samples is that the bundles are much tighter in the 750 °C sample so that some of the nanowires have amalgamated into one.

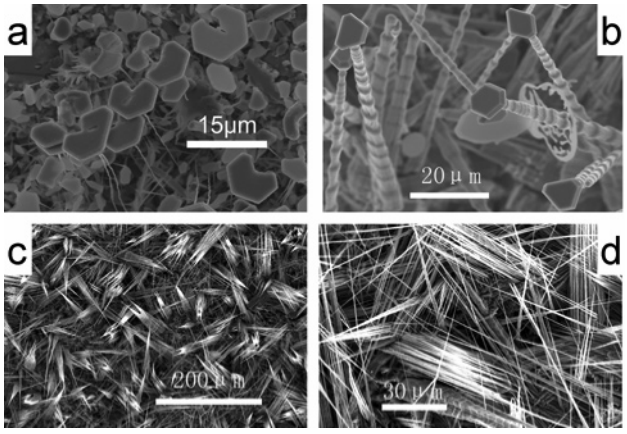

Figure 2. SEM images of featured samples 6−8 prepared at (a) 700, (b) 750, and (c) 800 °C. (d) Higher resolution image of c.

SEM II. SEM results of some featured samples (Nos. 6−8) are summarized in Figure 2. Both of the No. 6 (Figure 2a) and No. 7 (Figure 2b) samples are featured with the naillike products composed of slim nanowires and hexagonal plates, but also with some important differences. On one hand the nanowires in sample 6 have smooth surfaces, while the nanowires in sample 7 somewhat take the shape of towers. On the other hand the "hexagonal" plates in sample 6 are somewhat likely to be intermediates between those true hexagonal plates in sample 7 (Figure 2b) and the beltlike products in sample 3 (Figure 1f). The surface of the third featured sample (8; Figure 2c,d) is covered with lying bundles of nanowires.

XRD. SEM results have shown that there are four types of morphologies in all the samples, as the belt, the sheet, the hexagonal plate, and the nanowire. As mentioned above, Figure 1f shows that the belt and the sheet should have the same origin, and meanwhile Figure 2a shows that the hexagonal plate probably has the same origin with the belt. So the most typical morphologies left are the belt and the nanowire. Therefore although we have characterized all these samples with XRD, only two patterns are typical, as shown in Figure 3a (sample 1) and Figure 3b (sample 5), together with that of the lying nanowires (sample 8, Figure 3c). All of the reflections can be readily indexed to the hexagonal phase of Fe_7S_8 with lattice parameters: $a = b = 6.8673$ Å; $c = 17.062$ Å; space group, $P3_1$ (144) (JCPDS 71-0647). No peaks of any other phases or impurities were detected. So although the products are prepared at quite different conditions, they are chemically and crystallographically the same as 3C-Fe_7S_8. However, differences in the three patterns are apparent. The main difference between the patterns of the belt type (Figure 3a) and the nanowire type (Figure 3b) is the absence of the peaks ([0 0 3], [0 0 6], and [0 0 12] at the 2θ angles of 15.568, 31.434, and 65.608°, respectively) originated from the crystal growth along the *c*-axis in the former one. In addition, the main differences between the patterns of the lying nanowires (Figure 3c) and the nonlying sample (Figure 3b) are the almost absence of the peaks ([2 0 0], [2 2 0] at the 2θ angles of 30.027 and 53.318°, respectively) originated from the crystal growth perpendicular to the *c*-axis

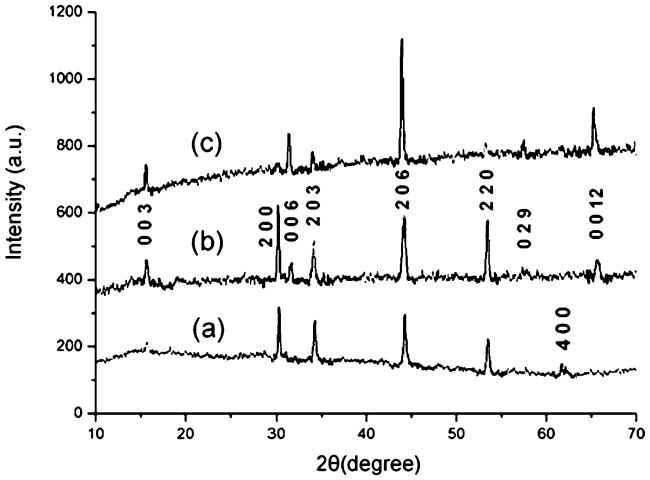

Figure 3. XRD patterns of representative samples: (a) beltlike products, sample 1; (b) nanowires, sample 5; and (c) lying bundles of nanowires, sample 8.

and the great enhancement of the peaks corresponding to the *c*-axis in the former one. Therefore we can safely deduce that the belt type (belt, sheet, and plate) is grown (almost) perpendicular to the *c*-axis, while the nanowire type prefers to grow (closely) along the *c*-axis.

TEM. TEM observations have provided more details about the samples. Although the beltlike network product (Figure 4a) takes an irregular shape, the selected area electron diffraction (SAED) pattern (Figure 4b) reveals that it is a single-crystal growing perpendicular to the *c*-axis. The unsymmetrical intensity of the spots in Figure 4b is originated from the irregular shape of the whole crystal. In addition the high-resolution TEM (HRTEM) image (Figure 4c) shows that the crystal is well-crystallized, almost free of defects except its interface with the amorphous sheath. Moreover, TEM results (Figure 4d,e) show that the hexagonal plate is also grown perpendicular to the *c*-axis, consistent with Xie's report.[10b] Thus the hexagonal plate does have the same origin with the belt. In contrast the nanowires are found to prefer to grow along the *c*-axis, as shown in Figure 4f−h. Energy-dispersive X-ray spectroscopy (EDS) investigations (see ESI) reveal that the sheaths are composed of SiO_2.

Discussion

In the former section we have reported colorful results obtained in our APCVD synthesis of silica-sheathed 3C-Fe_7S_8 products on silicon wafers with $FeCl_2$ and sulfur as the precursors. Four types of morphologies, as the hexagonal plate, the sheet, the belt, and the nanowire, are found. In this section we try to explain all these phenomena on the basis of the crystal structure of 3C-Fe_7S_8.

Chemistry. We have formerly discussed the main reactions in similar chemical systems in detail.[12b,14] Moreover we have attributed the formation of chemically stable species (metal sulfides and silica) in the final products to the extremely strong Si−O bonds.[14f] In addition we have deduced the adsorption of silica species on metal sulfides to be oxygen-bridged Si−(O)−metal−S type rather than sulfur-bridged O−Si−(S)−metal type, also on the basis of the extremely strong Si−O bonds.[14f] Obviously the same conclusion can be easily drawn in the chemical system discussed here (see also ref 15).

Freely Grown Fe_7S_8 Crystals. Before discussing the silica-sheathed Fe_7S_8 products, we first discuss the shape of freely grown Fe_7S_8 crystals. Figure 5a is a side elevation of atom distribution parallel to the (001) plane, while Figure 5b shows how atoms are distributed parallel to the (100) plane (crystal structure according to ref 16, room temperature data). Figure 5a shows that layers composed of four Fe atoms (Fe1, Fe2, Fe3, and Fe4, the 4Fe layer) and three iron atoms (Fe5, Fe6, and Fe7, the 3Fe layer) in unit cell alternatively appear along the *c*-axis; meanwhile the sequence perpendicular to the (100) plane shown in Figure 5b is more uniform, as 11−10−11−10 (may be defined as the 3.5Fe layer). Thus the growth along the *c*-axis should be alternatively fast (at the 4Fe layer) and slow (at the 3Fe layer), while the growth perpendicular to the *c*-axis should keep a steady and intermediate rate (see also details in ESI). This feature determines the dependence of the freely grown crystal shape on the temperatures. As long as the temperature is low, the 3Fe layer does not handicap the growth along the *c*-axis too much; hence, the crystals show no preferred growth direction, as demonstrated in Xie's reports.[10b] However when the temperature is high, this layer will cause great problems with the growth, and thus the crystal should be hexagonal plates, also in agreement with Xie's results. [10b]

Silica-Sheathed Products. Now that freely grown Fe_7S_8 crystals should either have no preferred growth directions or appear as hexagonal plates, our colorful results should be related to the silica sheath. Because the silica sheath tends to grow linearly[12b,14f] and the adsorption of vapor-phase silica species on existing silica sheaths is much easier than on Fe_7S_8 crystals, the initialization of silica-sheath formation on special surfaces of Fe_7S_8 crystals should determine the final shapes of the crystals. Accordingly we summarize the main aspects useful for the discussions on mechanisms in Figure 5c−e. We deem three main factors are responsible for the colorful results: Fe2−Fe3−Fe4 units, Fe2−Fe3−Fe6−Fe7 units, and kinetics.

Fe2−Fe3−Fe4 Units. First, Fe2, Fe3, and Fe4 (may be simply defined as Fe2−Fe3−Fe4 units) have the strongest bonds with S2 in the Fe_7S_8 crystal (see ESI). Therefore these iron atoms can have the strongest interactions with oxygen atoms. When the temperature is high or the vapor pressure of silica species is low, they should be the most preferred sites for the adsorption. This will result in preferred formation of silica sheaths on the (001) plane, and thus the products should be hexagonal plates.

Fe2−Fe3−Fe6−Fe7 Units. Second, other iron atoms should be taken into consideration when the vapor pressure of silica species turns higher. Iron atoms with interatomic distance of around 3 Å are highlighted in Figure 5c−e, because such distance provides the possible formation of an adsorbed cluster of one-silicon-atom-bridged two oxygen atoms bonded to two neighboring iron atoms (Fe−O−Si−O−Fe, adsorption of SiO_2). Such adsorption cluster includes the least number of adsorbed atoms required to form two bonds with the Fe_7S_8 crystal, and thus its adsorption should be less dependent on the vapor pressure of silica species. In addition, Fe2−Fe3−Fe6−Fe7 may form units especially favorable for the adsorption, because when one more oxygen atom is added to bond the two silicon atoms, a Si_2O_5 cluster, which has four O−Fe bonds with the Fe_7S_8 crystal, is formed. In comparison such Si_2O_5 cluster may be hardly formed on other four-iron-atom groups, for example Fe2−Fe3−Fe4−Fe1, due to strong tensions, because the silicon atoms should be sp^3 hybridized. So now we have singled out another unit favorable for the adsorption of silica species.

Kinetics. (1) Our model predicts the kinetic competition between adsorption on the 4Fe layer (Fe2−Fe3−Fe4−Fe1 units, taking Fe1 into consideration) and the Fe2−Fe3−Fe6−Fe7 units. As formerly pointed out, the Si_2O_5 cluster can hardly form

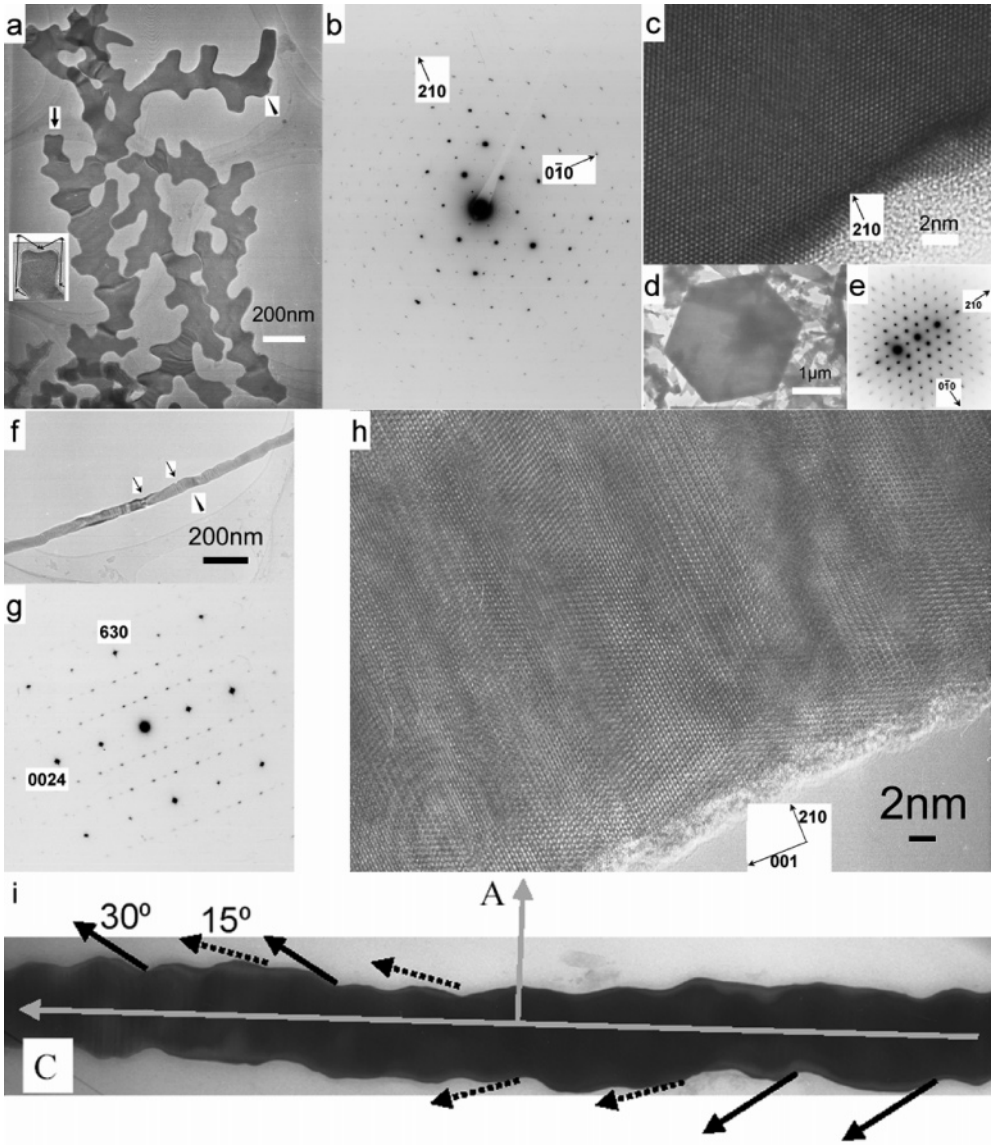

Figure 4. TEM characterization of representative samples. Beltlike products from sample 2: (a) low-resolution image; inset, higher resolution image of the region highlighted with the arrow in a (the group of arrows in the inset shows how the sheath is formed through bending with angles of 120 and 60°); (b) SAED pattern of the whole crystal; (c) HRTEM image of the region highlighted with the triangle in a. Hexagonal plate from sample 6: (d) crystal image; (e) SAED pattern (all the spots are originated from the interference between diffracted beams with the incident beam). Nanowires: (f) low-resolution image of a smoother nanowire (the two holes highlighted with the arrows are caused by the electron beam in EDS analysis); (g) SAED pattern; (h) HRTEM image of the region highlighted with the triangle in f; (i) sheath growth on a typical and rougher nanowire (two typical angles of sheath direction with that of the nanowire (*c*-axis) are highlighted with solid (30°) and dashed (15°) arrows, respectively).

on an Fe2−Fe3−Fe4−Fe1 unit; hence more atoms rather than one oxygen atom is required to connect the two neighboring SiO_2 (Fe−O−Si−O−Fe) clusters together so that a larger silica cluster is formed. Therefore although adsorption on the 4Fe layer is thermodynatically favorable when the adsorbed silica cluster is small, adsorption on the Fe2−Fe3−Fe6−Fe7 units will dominate in kinetics when the vapor pressure of silica species turns higher. The naillike products shown in Figure 2a,b, especially the towerlike nanowires in Figure 2b, are direct experimental proofs for such competition. (2) The 700 °C sample (3, Figure 1e,f) has shown silica-deficient behavior, and the products are predominantly nanosheets. Such behavior also occurs on a 750 °C sample (8, Figure 2c,d). The explanation lies in that higher vapor pressure is required to initialize the sheath formation when the temperature turns higher. In the meanwhile the reaction (between $FeCl_2$ and sulfur) speed is greatly accelerated. This should result in higher coverage of the silicon wafer, which serves as the silicon source for the silica sheaths, before the formation of the sheaths. Such kinetic competition may result in silica-deficient behavior at special experimental conditions.

Turning Angles. We can further predict the preferred turning angles of the sheaths on both the irregular beltlike products (Figure 4a) and the nanowires with rough surfaces (sample 5, Figure 4i) with our model. This only relates to the distribution of the Fe2−Fe3−Fe6−Fe7 units in the Fe_7S_8 crystals, as illustrated in Figure 5f. Supposing the turning angle is related to the next Fe2−Fe3−Fe6−Fe7 unit apart from the original sheath direction, the preferred turning angles should be 60 and 120° in the (001) plane according to Figure 5f. Experimental proofs can be easily found in Figure 4a (a higher resolution image is presented in ESI). And an example is highlighted in the inset of Figure 4a. For *c*-oriented nanowires, we illustrate two graphs in Figure 4g supposing we are viewing from the [120] or [010] direction. Turning with larger angles such as 45 and 48° meet the competition with the linear growth of the silica

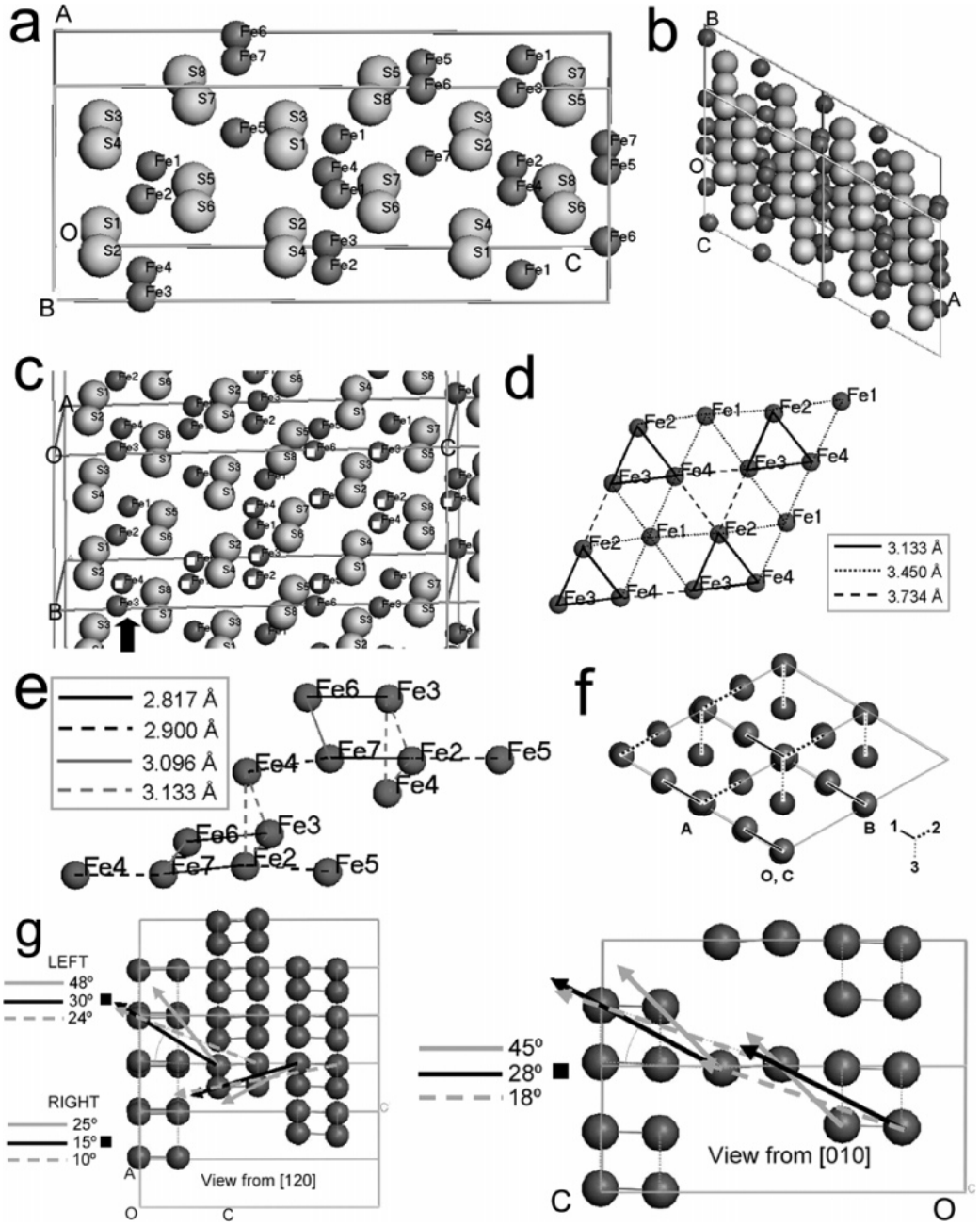

Figure 5. Fe_7S_8 crystal structure: (a) atom distribution along the *c*-axis; (b) atom distribution perpendicular to the *c*-axis; (c) two groups of iron atoms especially useful for sheath formation, highlighted with the black arrow and white squares, respectively; (d) interatomic distances between neighboring atoms in the 4Fe layer, as highlighted with the black arrow in c; (e) interatomic distances between neighboring atoms, as highlighted with white squares in c; (f) distribution of Fe2−Fe3−Fe6−Fe7 units along the *c*-axis (the numbers 1, 2, and 3 represent the units appearing consequently in the growth process along the *c*-axis; this indicates preferred turning angles of 60 and 120° of the sheath in the (001) plane); (g) possible turning angles of the sheath on a nanowire grown along the *c*-axis (the most preferred angles are about 15 and 28−30°, as highlighted with the black squares).

sheath. That is, silica species may adsorb on the protrusion of the core to form a new part of sheath growing along a new direction, but chances are better in this situation for them to bridge the protrusion with the nearby front of the sheath so that the sheath still grows linearly. While turning with 10, 24 (left part of Figure 4g), or 18° (right) has to run across more adsorption sites and thus are less favorable. Therefore the preferred turning angles are 15 and 28−30° on nanowires. Experimental proofs are shown in Figure 4i.

Special Results

Nanowires Synthesized at 650 °C. The above discussions have given a thorough explanation for all the experimental results shown in General Results. Especially we notice the possibility to prepare nanowires at 650 °C under elevated vapor pressure of the silica species, taking the advantage in kinetics of adsorption on Fe2−Fe3−Fe6−Fe7 units. Obviously such result will be a strong proof for our model. By introducing a trace amount of water into the system, we have succeeded in preparing naowires at 650 °C (sample 9). The SEM results are shown in Figure 6. HRTEM investigations indicate the nanowires are still Fe_7S_8 nanowires, but the silica sheaths turn to be much thicker, with typical thickness of 10 nm.

Ultralong Nanowires. Among the experimental results shown in General Results, the best sample of nanowires is sample 5 (Figure 1i,j). The typical wire length is only about 20−30 μm.

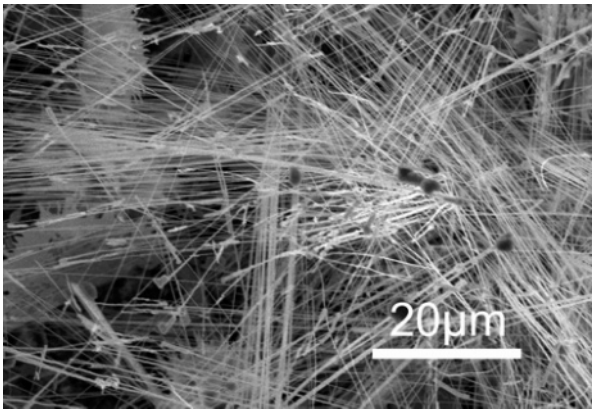

Figure 6. SEM image of nanowires prepared at 650 °C by introducing water into the system (sample 9).

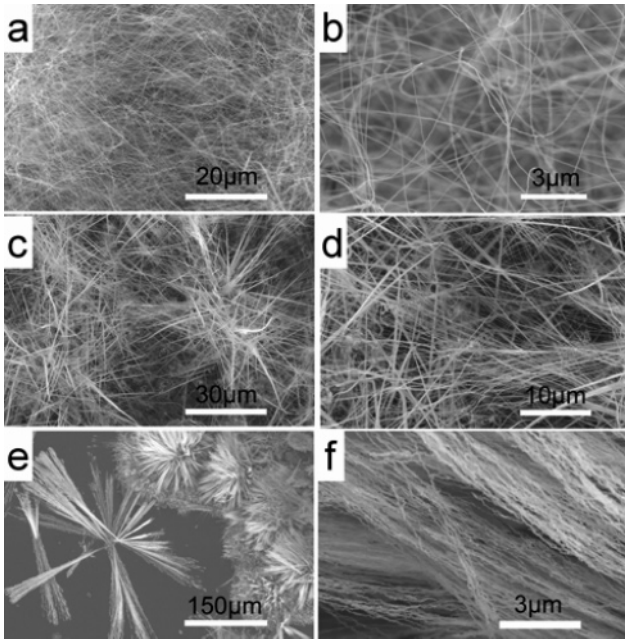

Figure 7. SEM images of nanowires on sample 10, at temperature regions of (a) 680, (c) 650, and (e) 620 °C. Higher resolution images of them are shown as b, d, and f, respectively.

Moreover, since the sample is prepared at 800 °C, thick film exists underneath the bundles of nanowires. To increase the ratio of nanowires in the final products and to prepare longer nanowires, we choose to put the silicon wafer at lower temperature region (620−680 °C) and lower the equivalent vapor pressure of $FeCl_2$ precursor. A small amount (0.10 g) of $FeCl_2 \cdot 4H_2O$ is put in the high-temperature region to initialize the sheath formation. SEM results of the sample (10) are summarized in Figure 7. At higher temperature region (680 °C, Figure 7a,b) the nanowires are so dense that we can hardly observe how they are originated from the silicon wafer. When the temperature turns lower (650 °C, Figure 7c,d), the nanowires appear as sparser bundles and some clusters are observed on the silicon wafer. At the lowest temperature region (620 °C, Figure 7e,f), clusters disappear. Meanwhile the bundles become sparser and ultralong nanowires (200−300 μm) are formed. Moreover the nanowires grown at higher temperature regions (Figure 7b,d) tend to have smoother surfaces in comparison with not only those grown at the lowest temperature region (Figure 7f) but also those synthesized at 800 °C (sample 5, Figure 1j). This phenomenon can also be explained on the basis of our model. As formerly discussed, the change on the sheath direction is related to the fastest grown 4Fe layer. On one hand, sample 10 is prepared by putting the crucible containing $FeCl_2 \cdot 4H_2O$ further away from the silicon wafer. Thus both precursors have to run through longer ways at the high-temperature region of the furnace. This will result in the formation of Fe_7S_8 clusters, which tend to expose the 3Fe layers rather than 4Fe layers. Such cluster-by-cluster types of growth significantly reduce the exposure time of 4Fe layers to silica vapor; thus the nanowires tend to have smoother surfaces. On the other hand, the growth rate of the 4Fe layer depends on temperature. Thus at low-temperature region, the exposure time should be longer; hence the nanowires turn to have rougher surfaces again.

Conclusions

In summary, we have systematically studied the synthesis of silica-sheathed Fe_7S_8 products in the temperature region of 600−800 °C. As a theoretical model, we single out the Fe2−Fe3−Fe4 units and the Fe2−Fe3−Fe6−Fe7 units as key structural factors determining the growth processes. Both theoretical investigations and experimental results have demonstrated the kinetic competition between the adsorption of silica species on the Fe2−Fe3−Fe4 units and the Fe2−Fe3−Fe6−Fe7 units has determined the morphology evolution at different experimental conditions.

Acknowledgment. This work was supported by NSFC (Grants 90406003, 20401010, 50372030, 20025102, and 20131030), the Foundation for the Author of National Excellent Doctoral Dissertation of the People's Republic of China and the state key project of fundamental research for nanomaterials and nanostructures (Grant 2003CB716901).

Supporting Information Available: XRD results of iron sulfide products obtained with anhydrous $FeCl_3$ precursor, details about the Fe−S bonds in 3C-Fe_7S_8, EDS spectra of a silica-sheathed Fe_7S_8 nanowire, and a higher resolution image of Figure 4a (PDF). This material is available free of charge via the Internet at http://pubs.acs.org.

References and Notes

(1) (a) Wang, Z. L.; Kong, X. Y.; Ding, Y. P.; Gao, X.; Hughes, W. L.; Yang, R. S.; Zhang, Y. *Adv. Mater.* **2004**, *16*, 943. (b) Ding, Y.; Ma, C.; Wang, Z. L. *Adv. Mater.* **2004**, *16*, 1740. (c) Ma, C.; Moore, D.; Li, J.; Wang, Z. L. *Adv. Mater.* **2003**, *15*, 228. (d) Li, F.; Ding, Y.; Gao, P. X.; Xin, X. Q.; Wang, Z. L. *Angew. Chem., Int. Ed.* **2004**, *43*, 5238. (e) Hughes, W. L.; Wang, Z. L. *J. Am. Chem. Soc.* **2004**, *126*, 6703. (f) Ding, Y.; Gao, P. X.; Wang, Z. L. *J. Am. Chem. Soc.* **2004**, *126*, 2066. (g) Yang, R. S.; Ding, Y.; Wang, Z. L. *Nano Lett.* **2004**, *4*, 1309. (h) Kong, X. Y.; Wang, Z. L. *Nano Lett.* **2003**, *3*, 1625. (i) Kong, X. Y.; Ding, Y.; Yang, R.; Wang, Z. L. *Science* **2004**, *303*, 1348.

(2) (a) Sun, Y. G.; Xia, Y. N. *Science* **2002**, *298*, 2176. (b) Sun, Y. G.; Mayers, B.; Herricks, T.; Xia, Y. N. *Nano Lett.* **2003**, *3*, 955. (c) Sun, Y. G.; Mayers, B.; Xia, Y. N. *Nano Lett.* **2003**, *3*, 675. (d) Sun, Y. A.; Xia, Y. N. *Adv. Mater.* **2003**, *15*, 695. (e) Mayers, B.; Xia, Y. N. *Adv. Mater.* **2002**, *14*, 279.

(3) (a) Peng, X. G.; Manna, L.; Yang, W. D.; Wickham, J.; Scher, E.; Kadavanich, A.; Alivisatos, A. P. *Nature* **2000**, *404*, 59. (b) Peng, Z. A.; Peng, X. G. *J. Am. Chem. Soc.* **2002**, *124*, 3343. (c) Peng, Z. A.; Peng, X. G. *J. Am. Chem. Soc.* **2001**, *123*, 1389. (d) Peng, X. G. *Adv. Mater.* **2003**, *15*, 459. (e) Jana, N. R.; Chen, Y. F.; Peng, X. G. *Chem. Mater.* **2004**, *16*, 3931. (f) Yu, W. W.; Wang, Y. A.; Peng, X. G. *Chem. Mater.* **2003**, *15*, 4300. (g) Puntes, V. F.; Krishnan, K. M.; Alivisatos, A. P. *Science* **2001**, *291*, 2115. (h) Manna, L.; Milliron, D. J.; Meisel, A.; Scher, E. C.; Alivisatos, A. P. *Nature Mater.* **2003**, *2*, 382. (i) Jun, Y. W.; Casula, M. F.; Sim, J. H.; Kim, S. Y.; Cheon, J.; Alivasatos, A. P. *J. Am. Chem. Soc.* **2003**, *125*, 15981.

(4) (a) Zeng, H.; Rice, P. M.; Wang, S. X.; Sun, S. H. *J. Am. Chem. Soc.* **2004**, *126*, 11458. (b) Hao, E. C.; Kelly, K. L.; Hupp, J. T.; Schatz, G. C. *J. Am. Chem. Soc.* **2002**, *124*, 15182. (c) Kim, Y. H.; Jun, Y. W.; Jun, B. H.; Lee, S. M.; Cheon, J. *J. Am. Chem. Soc.* **2002**, *124*, 13656. (d) Lee, S. M.; Jun, Y. W.; Cho, S. N.; Cheon, J. *J. Am. Chem. Soc.* **2002**, *124*, 11244. (e) Lee, S. M.; Cho, S. N.; Cheon, J. *Adv. Mater.* **2003**, *15*, 441. (f) Jana, N. R.; Gearheart, L.; Murphy, C. J. *Adv. Mater.* **2001**, *13*,

1389. (g) Yang, J.; Xue, C.; Yu, S. H.; Zeng, J. H.; Qian, Y. T. *Angew. Chem., Int. Ed.* **2002**, *41*, 4697. (h) Kanie, K.; Sugimoto, T. *Chem. Commun.* **2004**, 1584. (i) Leung, Y. H.; Djurisic, A. B.; Gao, J.; Xie, M. H.; Chan, W. K. *Chem. Phys. Lett.* **2004**, *385*, 155. (j) Zhou, Y.; Wang, C. Y.; Zhu, Y. R.; Chen, Z. Y. *Chem. Mater.* **1999**, *11*, 2310. (k) Chemseddine, A.; Moritz, T. *Eur. J. Inorg. Chem.* **1999**, 235. (l) Wang, Y.; Lee, J. Y.; Deivaraj, T. C. *J. Phys. Chem. B* **2004**, *108*, 13589. (m) Pillai, Z. S.; Kamat, P. V. *J. Phys. Chem. B* **2004**, *108*, 945.

(5) (a) Coey, J. M. D.; Roux-Buisson, H.; Brusetti, R. *J. Phys. (Paris)* **1976**, *37*, C4-1. (b) Townsend, M. G.; Gosselin, J. R.; Tremblay, R. J.; Webster, A. H. *J. Phys. (Paris)* **1976**, *37*, C4-11. (c) Gosselin, J. R.; Townsend, M. G.; Tremblay, R. J. *Solid State Commun.* **1976**, *19*, 799. (d) Shirai, M.; Suzuki, N.; Motizuki, K. *J. Electron Spectrosc. Relat. Phenom.* **1996**, *78*, 95. (e) Kobayashi, H.; Sato, M.; Kamimura, T.; Sakai, M.; Onodera, H.; Kuroda, N.; Yamaguchi, Y. *J. Phys.: Condens. Matter* **1997**, *9*, 515. (f) Becker, U.; Munz, A. W.; Lennie, A. R.; Thornton, G.; Vaughan, D. J. *Surf. Sci.* **1997**, *389*, 66.

(6) (a) Ennaoui, A.; Fiechter, S.; Pettenkofer, Ch.; Alonso-Vante, N.; Büker, K.; Bronold, M.; Höpfner, Ch.; Tributsch, H. *Sol. Energy Mater. Sol. Cells* **1993**, *29*, 289. (b) Bither, T. A.; Bouchard, R. J.; Cloud, W. H.; Donohue, P. C.; Siemens, W. J. *Inorg. Chem.* **1968**, *7*, 2208.

(7) (a) Horwood, J. L.; Townsend, M. G.; Webster, A. H. *J. Solid State Chem.* **1976**, *17*, 35. (b) Hirahara, E.; Murakami, M. *Phys. Chem. Solids* **1958**, *7*, 281. (c) Li, E.; Franzen, H. F. *J. Solid State Chem.* **1996**, *126*, 108. (d) O'Reilly, W.; Hoffmann, V.; Chouker, A. C.; Soffel, H. C.; Menyeh, A. *Geophys. J. Int.* **2000**, *142*, 669. (e) Takele, S.; Hearne, G. R. *J. Phys.: Condens. Matter* **2001**, *13*, 10077. (f) Shimada, K.; Mizokawa, T.; Mamiya, K.; Saitoh, T.; Fujimori, A. *Phys. Rev. B* **1998**, *57*, 8845. (g) Zapletal, K. *Phys. Earth Planet. Inter.* **1992**, *70*, 302.

(8) Dunlop, D. J.; Özdemir, Ö.; Clark, D. A.; Schmidt, P. W. *Earth Planet. Sci. Lett.* **2000**, *176*, 107.

(9) (a) Montoro, L. A.; Rosolen, J. M. *Solid State Ionics* **2003**, *159*, 233. (b) Ennaoui, A.; Fiechter, S.; Tributsch, H.; Giersig, M.; Vogel, R.; Weller, H. *J. Electrochem. Soc.* **1992**, *139*, 2514.

(10) (a) Nath, M.; Choudhury, A.; Kundu, A.; Rao, C. N. R. *Adv. Mater.* **2003**, *15*, 2098. (b) Xie, Y.; Zhu, L. Y.; Jiang, X. C.; Lu, J.; Zheng, X. W.; He, W.; Li, Y. Z. *Chem. Mater.* **2001**, *13*, 3927. (c) Xu, X. Y.; Li, X. G. *Chin. Chem. Lett.* **2003**, *14*, 83. (d) Dörr, M.; Petzold, H.; Kreisel, G.; Völksch, G.; Weigand, W. *Z. Anorg. Allg. Chem.* **2003**, 629, 1113.

(11) Qian, X. F.; Zhang, X. M.; Wang, C.; Xie, Y.; Wang, W. Z.; Qian, Y. T. *Mater. Sci. Eng., B* **1999**, *64*, 170.

(12) (a) Shyu, S. G.; Wu, J. S.; Wu, C. C.; Chuang, S. H.; Chi, K. M. *Inorg. Chim. Acta* **2002**, *334*, 276. (b) Ge, J. P.; Wang, J.; Zhang, H. X.; Li, Y. D. *Chem.−Eur. J.* **2004**, *10*, 3525.

(13) (a) Bouchard, R. J. *J. Cryst. Growth* **1968**, *2*, 40. (b) Ennaoui, A.; Schlichtlorel, G.; Fiechter, S.; Tributsch, H. *Sol. Energy Mater. Sol. Cells* **1992**, *25*, 169. (c) Bronold, M.; Kubala, S.; Pettenkofer, C.; Jaegermann, W. *Thin Solid Films* **1997**, *304*, 178. (d) Meester, B.; Reijnen, L.; Goossens, A.; Schoonman, J. *Chem. Vap. Deposition* **2000**, *6*, 121. (e) Schleigh, D. M.; Chang, H. S. W. *J. Cryst. Growth* **1991**, *112*, 737. (f) Thomas, B.; Höpfner, C.; Ellmer, K.; Fiechter, S.; Tributsch, H. *J. Cryst. Growth* **1995**, *146*, 630. (g) Höpfner, C.; Ellmer, K.; Ennaoui, A.; Pettenkofer, C.; Fiechter, S.; Tributsch, H. *J. Cryst. Growth* **1995**, *151*, 325. (h) Thomas, B.; Cibik, T.; Höpfner, C.; Diesner, K.; Ehlers, G.; Fiechter, S.; Ellmer, K. *J. Mater. Sci.* **1998**, *9*, 61. (i) Smestad, G.; Silva, A. da; Tributsch, H.; Fiechter, S.; Kunst, M.; Meziani, N.; Birkholz, M. *Sol. Energy Mater.* **1989**, *18*, 299. (j) Smestad, G.; Ennaoui, E.; Fiechter, S.; Tributsch, H.; Hofman, W. K.; Birkholz, M. *Sol. Energy Mater.* **1990**, *20*, 149. (k) Ferrer, I. J.; Sanchez, C. *J. Appl. Phys.* **1991**, *70*, 2641. (l) Bausch, S.; Sailer, B.; Keppner, H.; Willeke, G.; Bucher, E.; Frommeyer, G. *Appl. Phys. Lett.* **1990**, *57*, 25. (m) Rezig, B.; Dalman, H.; Kanzai, M. *Renew. Energy* **1992**, *2*, 125.

(14) (a) Ge, J. P.; Li, Y. D. *Chem. Commun.* **2003**, 2498. (b) Ge, J. P.; Li, Y. D. *Adv. Funct. Mater.* **2004**, *14*, 157. (c) Li, X. L.; Ge, J. P.; Li, Y. D. *Chem.−Eur. J.* **2004**, *10*, 6163. (d) Ge, J. P.; Wang, J.; Zhang, H. X.; Wang, X.; Peng, Q.; Li, Y. D. *Adv. Funct. Mater.* **2005**, *15*, 303. (e) Ge, J. P.; Wang, J.; Zhang, H. X.; Wang, X.; Peng, Q.; Li, Y. D. *Chem.−Eur. J.* **2005**, *11*, **1889**. (f) Zhang, H. X.; Ge, J. P.; Li, Y. D. *Chem. Vap. Deposition* **2005**, *11*, **147**. (g) Ge, J. P.; Wang, J.; Zhang, H. X.; Wang, X.; Peng, Q.; Li, Y. D. *Sens. Actuators, B*, in press.

(15) Prabhakaran, K.; Watanabe, Y.; Nath, K. G.; Homma, Y.; Ogino, T.; Shafi, K. V. P. M.; Ulman, A. *Surf. Sci.* **2003**, *545*, 191.

(16) Fleet, M. E. *Acta Crystallogr., Sect. B: Struct. Crystallogr. Cryst. Chem.* **1971**, *27*, 1864.